Simulating human fingers: a Soft Finger Proxy Model and Algorithm

Federico Barbagli [†*], Antonio Frisoli [§], Kenneth Salisbury [†], Massimo Bergamasco[§]

[†] Stanford University - Robotics Lab
Stanford, CA, U.S.A. - [barbagli,jks]@robotics.stanford.edu
[§] PERCRO - Scuola Superiore S.Anna
Pisa, Italy [antony,bergamasco]@sssup.it
[*] DII - University of Siena - Siena, Italy

Abstract

This paper presents models and algorithms that can be used to simulate contact between one or more fingertips and a virtual object. First, the paper presents various models for rotational friction obtained from in-vivo fingertip models previously proposed in the robotics and biomechanics community. Then the paper describes two sets of experiments that were performed on in-vivo fingertips in order to understand which of the models presented fits best with the real rotational friction properties of the human fingertips. Finally an extension of the god object/proxy algorithm which allows the simulation of soft finger contact, i.e. a point-contact with friction capable of supporting moments (up to a torsional friction limit) about the contact normal, is proposed. The resulting algorithm is computationally efficient, being point-based, while retaining a good level of realism.

1. Introduction and motivation

One of the key features of the human fingertips is to be able to resist moments, up to a torsional friction limit, about contact normals. This simple, and yet essential feature, allows humans to fully restrain objects using two fingertips, something that would be impossible to do using the tip of two tools. As new haptic devices allowing interaction through multiple points of contact are being created [1, 2], it is essential to be able to simulate this type of contact in order to support tasks such as virtual grasping. Haptic rendering algorithms simulating point-contact, such as the proxy [16] and the god-object [22], have been popular for a decade thanks to their computational efficiency, but fail to model the rotational friction capabilities of the human fingertip. The focus of this paper is to present a haptic rendering algorithm that simulates human fingertip capabilities while preserving computational efficiency of point-based algorithms.

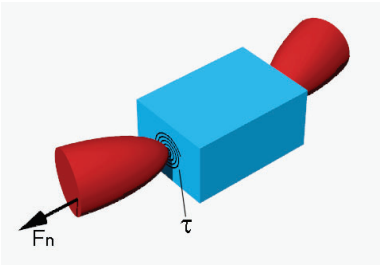

Figure 1. By using two soft finger proxies subjects can fully restrain a virtual object.

The paper first presents various models for rotational friction obtained from in-vivo fingertip models previously proposed in the robotics and biomechanics community (see section 4). Two sets of experiments that we performed on in-vivo fingertips, in order to understand which of the models presented fits best with the real rotational friction properties of the human fingertips, are then presented (see section 5). Finally an algorithm which extends the proxy and god-object capabilities to include rotational friction constraints is presented (see section 8). The algorithm is called soft-finger proxy in reference to the soft-finger contact used in the robotic grasping community [17].

As it turns out, while one of the four proposed models matches the overall human fingertip properties better than the other three, this can be ignored in the case of point-based algorithms such as the one proposed in this paper, for which the contact surface area is not considered.

2. State of the art for in-vivo fingertip models

The robotics community has proposed various models of frictional properties for robotic fingertips in the past two decades [3, 9, 10].

The Neuroscience community, mainly in the form of Professor Johansson's group, has studied frictional properties of human fingertips in order to evaluate what are the minimal forces applied by humans in order to stably grasp objects [21] and to resist tangential torques, i.e. to restrain objects from rotating using rotational friction [12, 5]. The main results of such researches is that in both cases the normal force that is applied by subject in order to resist tangential force and torques is always the minimal amount that ensures avoiding slippage. Moreover the ratio between normal force and tangential torque, and normal force and tangential forces is always linear. In [12] the authors propose three functions to model the slip force on the basis of tangential torque and normal force applied to the object. All of the proposed models fit experimental data obtained by the authors well but none of them is based on any theoretical model of the human fingerpad.

In recent years the bio-mechanical community has proposed various mathematical models that closely simulate the force-displacement and force-contact area behavior of in-vivo fingertips [20, 18, 19, 15, 14]. Note that none of these papers present results concerning frictional properties of the human fingerpad.

3 Basic assumptions

Some basic assumptions, typically adopted by existing literature on human fingerpad modelling, are maintained in this paper. The fingerpad is modelled as a sphere, the contact area is assumed to be a circle of radius a, and the pressure distribution is assumed to be axial-symmetric.

Under the effect of contact force P, a distribution of pressure $p(r)$ is generated over the contact area, such that:

$$P = \int_0^a p(r) 2\pi r dr \tag{1}$$

Under static conditions, friction forces depend on the friction coefficient μ. In such case p produces on a infinitesimal area dA a tangential traction q such that:

$$|q| \leq \mu p \, \mathrm{dA} = F_{fr} \tag{2}$$

The local values of F_{fr} determine the conditions for which slip between the two bodies in contact can occur, and generate a friction moment M given by:

$$M = \int_0^a \mu p(r) 2\pi r^2 dr = P r_m(a) \tag{3}$$

with

$$r_m(a) = \frac{\int_0^a \mu p(r) r^2 dr}{\int_0^a p(r) r dr} \tag{4}$$

Equations (1) and (3) are assumed to hold independently of the mathematical model adopted for the fingerpad.

Following [11], the kinematic equation governing the deformation of the two surfaces in contact can be derived by studying the displacement of two points $S_1(x, y, z_1)$ and $S_2(x, y, z_2)$, belonging respectively to the surface of body 1 and 2. In the unloaded case the two points S_i are assumed to be separated by a distance h.

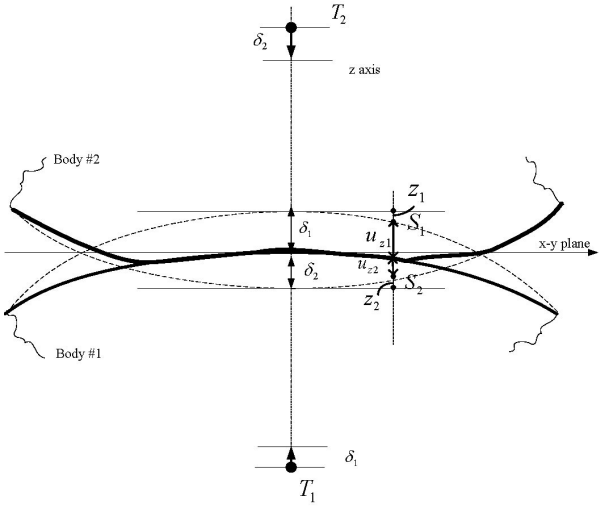

Figure 2. Elastic contact of two bodies.

Referring to Figure 2, let us consider two points T_1 and T_2, located on the $z-$axis far apart from the contact region. Any relative contact motion of δ between the two bodies can be expressed as a combination of motions of points T_1 and T_2 of amounts δ_1 and δ_2, such that $\delta = \delta_1 + \delta_2$. As the two bodies deform the position of each point S_i belonging to the contact area can be described by:

$$u_z + h = \delta \tag{5}$$

with $u_z = u_{z1} + u_{z2}$. In order to fully describe the contact problem between to generic elastic bodies we will solve relationship 5, which represents the geometric constraint equation for the contact, as well as a constitutive equation relating contact forces and displacements. The latter relationship depends on the particular mechanical structure of the bodies in contact while the former does not.

4 Contact deformation models

This section presents four possible models for the human fingerpad. The goal is to obtain an analytical relationship

describing the frictional properties of each of these models. The first two models (Classic Hertz - CH, Modified Hertz - MH) are based on Hertzian theory (see [3] for CH and [15, 14] for MH). The third model (Viscous Sphere - VS), which was originally used to describe the behavior of plantar soft tissue, is based on a viscous sphere representation (see [7]). The fourth model (Liquid Filled Membrane - LFM) describes the fingerpad as a fluid filled membrane (see [19]).

These four models feature different constitutive equation and thus different rotational friction properties. Such properties will be derived in the following.

4.1 Classic Hertzian model

For the CH model of a fingerpad, which was determined by Brock et al. in [3], contact with a given surface is approximated as one between two elastic solids, and thus can be described using Hertzian theory [8]. The geometric constrain equation for the CH model is given by:

$$a^2 = R\delta \tag{6}$$

The resultant distribution of pressure over the contact area has an elliptical shape described by

$$p = p_0[1 - (\frac{r}{a})^2]^{1/2} \tag{7}$$

and the radius of the contact circle depends on the applied force P through equation

$$a = \frac{\pi p_0 R}{2E^*} \tag{8}$$

By using (1) and (3) the expressions for the contact force P and the friction moment M are found as:

$$P = \int_0^a p(r)2\pi r dr = \frac{2}{3}p_o \pi a^2 \tag{9}$$

$$M = \int_0^a \mu p(r)2\pi r^2 dr = \frac{2\pi p_0}{a}\mu \int_0^a \sqrt{a^2 - r^2} r^2 dr = \tag{10}$$

$$= \mu \frac{2\pi p_0}{a}\frac{a^4\pi}{16} = \frac{1}{8}\mu p_0 a^3 \pi^2 \tag{11}$$

and thus

$$\frac{M}{P} = \frac{3\pi}{16}\mu a(P) \tag{12}$$

4.2 Modified Hertzian model

In [15], Howe et al. proposed a modification of the classic hertzian model to fit the indentation displacement vs. force curve obtained using measures made through tactile sensors. Two corrective terms, the experimental instantaneous response T_e and the relaxation response, were introduced. For our purposes, if relaxations effects are neglected, we can modify expression (7) of p to only include T_e, and thus obtain[1]

$$p'(r) = p(r)T^e(\delta) \tag{13}$$

It can be shown that under this hypothesis the expression of the ratio M/P remains unchanged and equal to (12). Moreover by using (8) and (19), classic Hertzian theory predicts that

$$a = \frac{3\pi}{16}P\left(\frac{3PR}{4E^*}\right)^{1/3} \tag{14}$$

4.3 Viscous sphere (VS) model

In the formulation of hertzian model given in equation (6), it was implicitly assumed that the contact geometry can be described by looking only at a close neighborhood of the contact point, and this is valid only for infinitesimal deformations. When finite deformations are taken into account, i.e. when the entity of displacement due to the contact deformation is not negligible with respect to the nominal dimension of the fingerpad, this assumption is no longer valid. In this section we present a model inspired by a previous work [7] that includes the case of finite deformation.

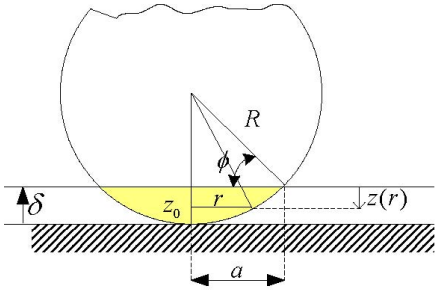

Figure 3. Contact of a viscoelastic sphere over a plane

Referring to Figure 3, we will assume that, during contact, points on the sphere surface will be displaced of a quantity equal to their distance from the plane in the undeformed configuration. The geometric constrain equation for this model is given by

$$(R - \delta)^2 + a^2 = R^2 \tag{15}$$

where displacement $z(r)$ is given by

$$z(r) = \sqrt{R^2 - r^2} - \sqrt{R^2 - a^2} = \sqrt{R^2 - r^2} - R + \delta \tag{16}$$

[1] Note that equation (8) is not completely compatible with the mathematical formulation of the *problem of the plane* (see Appendix 1), of which it represents an approximate solution only.

We will suppose that the state of stress induced by the contact can be modelled through the effect of multiple springs, with finite displacements, acting only along the normal to the plane. As a consequence, the pressure distribution is described by $p(r) = kz(r)$, and results in a contact force

$$P = \int_0^a p(r) 2\pi r dr = \frac{1}{3}\pi k \delta^2 (3R - \delta) \qquad (17)$$

where, in order to model each spring element in a non-linear way, the elastic constant is given by $k = k'\delta^n$. The friction moment is given by

$$M = \int_0^a \mu p(r) 2\pi r^2 dr = \mu\pi k[(R-\delta)a(R^2/4 - 2/3a^2) - a/2(R^2 - a^2)^{3/2} + R^4/4\phi)] \qquad (18)$$

Since generally the values of M/μ are computed numerically, the relationship between M/μ_m vs. P can be described through an approximating function of (18) in the range of values of interest.

4.4 Liquid filled (LF) membrane

Serina et al. [19] adopted a structural model for fingertip pulp based on the theory of elastic membranes [6]. While this model allows the representation of large strain deformations, it has the limitation of only admitting reaction forces tangential to the surface aligned along circumferential and tangential directions. This implies that the distribution of pressure during contact is uniform and given by internal pressure p.

In this case P and M are given by

$$P = \int_0^a p 2\pi r dr = \pi p_0 a^2 \qquad (19)$$

$$M = \int_0^a \mu p(r) 2\pi r^2 dr = \frac{2}{3}\mu\pi p_0 a^3 \qquad (20)$$

and thus

$$\frac{M}{P} = \frac{2}{3}\mu a(P) \qquad (21)$$

Where $a(P)$ has been obtained from experimental measures reported in [19].

5. Experimental measure of human fingerpad characteristics

In order to evaluate which of the models presented in section 4 better matches the real behavior of in-vivo human fingertip, experimental data was obtained and analyzed. More specifically, three relationships were considered when comparing experimental data with analytical models of the human fingertip:

E1. Relationship P vs. δ between normal force and normal displacement.

E2. Relationship P vs. a between normal force and radius of the contact area.

E3. Relationship M vs. P between friction moment and normal force.

This section describes how these experimental measures of human fingerpad characteristics have been derived. Such experimental data is then used in section 6 to fit models proposed in section 4.

5.1 E1: Measures of the indentation displacement

For relationship E1 we will consider the results proposed by Howe et al. in [15], where the authors suggest that instantaneous elastic indentation force can be modelled through an exponential formulation:

$$P = T^e(\delta) = \frac{b}{m}(e^{m(\delta - \delta_0)} - 1) \qquad (22)$$

where $\delta_0 = 0\,\text{mm}$, $b = 0.19\,\text{N/mm}$ $m = 2.1\,\text{mm}^{-1}$.

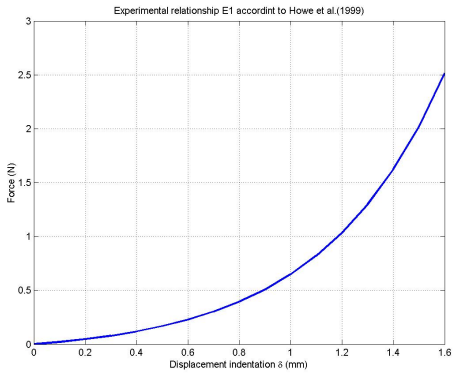

Figure 4. Experimental P vs. δ relationship.

5.2 E2: Measures of the contact area

Experimental measures of the contact area vs. normal force have been reported by other authors, e.g. see [18, 19], but never reported in analytical form. The results presented here, which were conducted using the procedure proposed in [18], confirm the results previously found.

Two healthy right-handed men served as subjects for this study. All of the subjects gave their informed consent to participate in the experiment. The experimental apparatus was made of a sheet of white paper placed on a metal plate

which was fixed to a one degree of freedom load cell. During each trial subjects were asked to stain their index fingerpad with black ink and then press on the paper sheet holding the finger at approximately $0°$. Forces normal to the paper sheet were recorded. Paper sheets were substituted between different trials.

At the end of all trials paper sheets were digitally scanned. The magnitude A of the contact area was estimated for each digital image using the Matlab Image processing toolbox, and the equivalent contact radius $a = \sqrt{\frac{A}{\pi}}$ was derived. Each radius was then matched to the peak force measured during the relative trial.

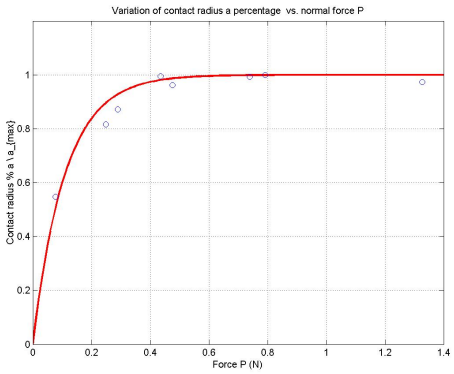

Figure 5. Experimental P vs. a/a_{max} relationship.

From the analysis of experimental data it is possible to assume the following model describing a

$$\frac{a}{a_{max}} = (1 - e^{(-P/P_0')}) \tag{23}$$

where a_{max} is the peak value for the radius of the user's finger and where $P_0' = 0.1101\,N$ provides the best quadratic fit. Figure 5 shows the variation of a/a_{max} with respect to P.

5.3 E3: Measure of friction coefficient

Five healthy right-handed men with average age of 28 served as subjects for this study. All of the subjects gave their informed consent to participate in the experiment. Subjects sat on a height adjustable chair with their left arm extended anteriorly. The subjects' forearm rested on a wood block in order to prevent fatigue from having to hold their hand in a same position for a prolonged time. The block's height was chosen in order for all experiments to be carried out with the finger forming a $0°$ angle with the testing apparatus.

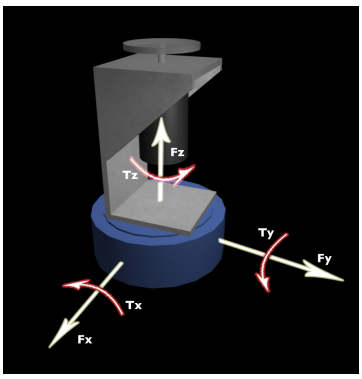

Figure 6. Schematic 3D model of the apparatus and the coordinate system for measured forces and torques.

The apparatus shown in Figure 6 was used for measuring the relationship between load force and friction moment and thus evaluate coefficients of static friction. The experimental apparatus was made of a six degrees of freedom load cell (labelled d) (JR3 Force-Moment sensor model 67M25A-U560, JR3 Multi-Axis Load Cell Technologies, Woodland, CA), a 35 mm DC motor (c) (Maxon DC motor 137562 35mm, Maxon Precision Motors, Switzerland) mounting an optical encoder (Maxon HEDL-5540 A11, Maxon Precision Motors, Switzerland) and a metal casing (e) built in order to support the motor vertically above the geometrical center of the force sensor. Thus, referring to Figure 6, the F_z axis intersects the sensor's geometrical center and is the axis of rotation for the DC motor and its shaft. The metal structure was rigidly fixed to the force sensor as well as to the motor. Plates made of different materials (a) could be fixed at the tip of the motor shaft (b), which was free to rotate through an opening in the metal structure described above. The geometrical center of each plate was intersected by axis F_z. A square-shaped borosilicate glass plate mounting a sorbothane ultra-soft polyurethane sheet ($3/8''$-thick with a surface of $2'' \times 2''$ was used for the experiments.

Force range were of 126 Newton along the z axis, of 63 Newton along the x and y axis and of 4 Newton-meter on all the three torque components, with resolution of $1/4000$ over the full sensor range. The motor position resolution was $0.18\,\mathrm{deg}$. Data was read from both force sensor and motor with a 1KHz servo-rate. Force data was read using a JR3 ISA I/O board. Position of the motor's shaft was read using a Sensoray 626 PCI board. All the software used to run the experiments was written using the Borland C++ builder and the *chai3d* libraries. Each experiment was made up of 80 trials. Throughout each trial a constant torque was commanded to the motor. The value of such torque was changed between trials. Torques were varied between nom-

inal values ranging from 0 Nm to 1 Nm.

At the beginning of each trial the subject was asked to place his/her left-hand index fingerpad in the geometric center of the plate connected to the motor shaft while the motor was not moving. When the subject was ready a constant torque was commanded to the motor. The subject was asked to press on the plate in order to stop the plate through the fingerpad rotational friction. Once an equilibrium was reached and the plate's velocity was zero the recording phase began. Load applied by the subject, reaction torque and motor velocity were recorded. The subject was asked to slowly decrease the load force. Once slippage was detected the recording phase lasted for five additional seconds and then the motor was brought to a stop. Between each trial, the subject was instructed to wait 1.5 minutes before starting the next trial. This precaution was necessary in order to allow the finger pulp to restore to its natural shape.

By inspecting the data obtained in experiments carried out an average relationship between r_m and P was found, for the rubber plate, as shown in Figure 7.

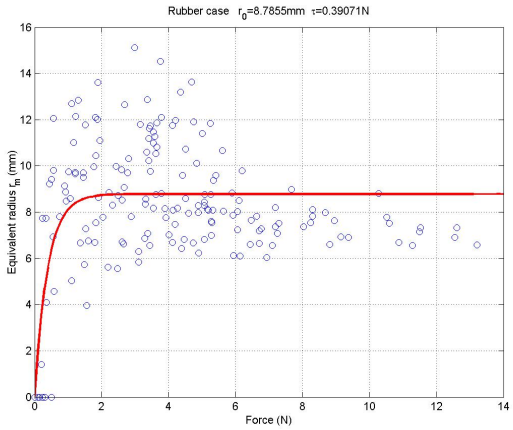

Figure 7. Experimental P vs. r_m relationship

Such relationship can be analytically modelled as

$$r_m = r_0(1 - e^{(-P/\tau)}) \tag{24}$$

where $r_0 = 8.7855\,mm$ and $\tau = 0.3907\,N$ provide the best quadratic fit. The values of r_m are always bounded by the values of a, i.e. they can never exceed the maximum dimension of the fingerpad, as can be seen by the following inequality

$$r_m(a) < \mu \frac{\int_0^a p(r) r^2 dr}{\int_0^a p(r) r dr} = \mu a \frac{\int_0^a p(r) r dr}{\int_0^a p(r) r dr} = \mu a \tag{25}$$

Relationship E3 between M and P has been computed using 3. The results are plotted in Figure 8.

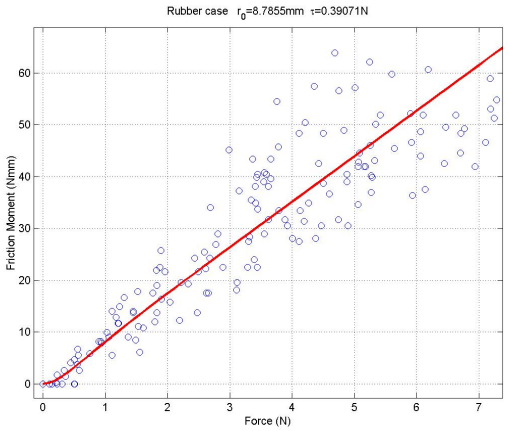

Figure 8. Experimental P vs. M relationship.

6 Fitting of the proposed models

In the following the human fingerpad models presented in section 4 will be compared with the experimental curves obtained in section 5.

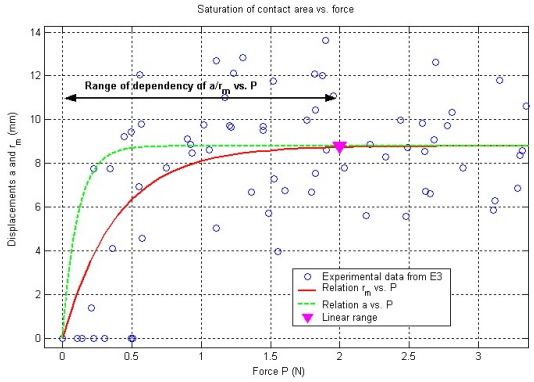

Figure 9. The effect of saturation M vs. normal force P

From the analysis of the experimental data relative to laws E2 and E3 it can be noticed how the dependency of M vs. P is almost linear for great values of force P. Non-linear effects due to the geometry of contact are evident only for small indentation displacements. The range of forces P which affect the dimension of the contact area a and of the friction equivalent radius r_m is equal to $0-2N$, as presented in Figure 9. Beyond this range of values, the contact area reaches its maximum value and relationship E3 between M and P can be considered linear.

In the following we will examine which of the models presented better fits the non-linear relationship between M

and P in the $0-2N$ range. In general we will assume that such relationship has the following form

$$M = \begin{cases} \mu'_m P^n & \text{if } 0 < P < P^* \\ \mu_m (P - P^*) + \mu'_m P^{*n} & \text{if } P > P^* \end{cases} \quad (26)$$

Clearly in order to guarantee the continuity of first derivative of M at point P^* it must hold for $P = P^*$:

$$\mu'_m n P^{*n-1} = \mu_m \quad (27)$$

The value of μ is equal to r_0 in (24), since it represents the slope of the linear part of the experimental relationship of E3. The value of n will depend on the specific mathematical model adopted for the description of the contact in the non-linear range. Once n is known, from (27) it is then possible to determine the value of μ'_m. In the following estimated values for coefficient n are presented for all four mathematical models previously introduced.

6.1 CH model

For the classical Hertzian model CH, the relationship between M and P only depends on $a(P)$, and thus by substituting expression (14) in (12), we find

$$M = \frac{3\pi}{16}\mu a P = \frac{3\pi}{16}\mu P \left(\frac{3PR}{4E^*}\right)^{1/3} = \quad (28)$$

$$= \frac{3\pi}{16}\mu \left(\frac{3R}{4E^*}\right)^{1/3} P^{4/3} = \mu'_m P^{4/3} \quad (29)$$

The P vs. M relationship for the Classic Hertz (CH) model is thus obtained as

$$M = \mu'_m P^{1.3333} \quad (30)$$

6.2 MH model

In the non-linear range relationship (22) can be expressed as

$$P(\delta) = p_1 \delta^{p_2} \quad (31)$$

where the values of coefficients

$$p_1 = 0.5118 \frac{\text{N}}{\text{mm}^{p_2}}, \; p_2 = 3.4897 \quad (32)$$

have been found as the ones that minimize the L^2 norm of functions (32) and (22) in the non-linear range of forces $0-2N$. From (32) it is possible to determine

$$P(a) = \frac{p_1}{R^{3.4897}} a^{6.9795} \quad (33)$$

and combining this equation with (12), the Modified Hertz (MH) model law is obtained as

$$M = \mu'_m P^{1.1433} \quad (34)$$

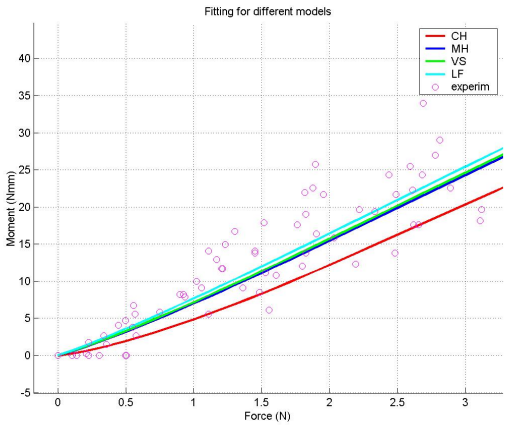

Figure 10. Fitting of presented models for the M vs. P relationship in the $0-2N$ range of normal forces.

6.3 VS model

Values of k' and n in (17) can be determined as the ones that best fit the experimental law E1 presented in (22) using an L_2 norm. The values obtained $k' = 0.0242$ and $n = 1.5753$, lead to an approximating function of the form (26) given by

$$M = 2.3286 \mu P^{1.1289} = \mu_m P^{1.1289} \quad (35)$$

where all the numeric constants have been included within the friction coefficient μ_m.

6.4 LF model

We assume that the liquid filled membrane model matches with both displacement δ and area deformation a versus force P experimental plots as reported by [19].

As for the law E1, an equivalent expression in the non-linear range of relationship E2, presented in given by (23), can be converted in power formulation

$$a(\delta) = q_1 P^{q_2} \quad q_1 = 0.9809 \frac{\text{mm}}{\text{N}^{q_2}}, \; q_2 = 0.0949 \quad (36)$$

The unknown coefficients q_1 and q_2 have been found as the ones that minimize the L^2 norm of the two functions over the interval 0-2 N. By substituting the expression of (36) into the (21), the M vs. P relationship becomes

$$M = \mu'_m P^{1.0949} \quad (37)$$

6.5 Discussion

The values of μ'_m determined are reported in table 6.5, where torques are expressed in Nmm while forces in N.

All models have been tuned to fit the M vs. P relationship (E3) and the P vs. δ relationship (E1). However, not all models fit the P vs. a relationship (E2) equally well. In the past section we have assumed that, in accordance to what has been reported in [19], the LF model perfectly matches both P vs. a and P vs. δ relationships. As a consequence the LF model is the closest to fit all three sets of experimental data.

An important note is, however, that often the contact area may not be of interest in a simplified haptic rendering algorithm, as in the case of the algorithm proposed in this paper. In such case any of the proposed models can be used since the relationship between M and P is similar in each of the four cases for the range of forces under study.

model	μ'_m
CH	8.1489
MH	8.8327
VS	8.8836
LFM	9.0028

Table 1. Values of global friction coefficient μ_m found in different models

7. The extended soft-finger proxy algorithm

In what follows we will propose a soft-finger proxy algorithm. It is important to note that friction models to be used in haptic simulation have been proposed in the past by various research groups (see [22, 16, 4, 13] amongst others). To the authors' knowledge, however, none of such models have been applied to simulate rotational friction.

In order to simulate a soft finger contact a 4 DOF proxy can be used. Three of such degrees of freedom describe the position that the point of contact would ideally have when touching a virtual object (as for the standard proxy algorithm). The fourth variable describes the relative angular motion between the two soft finger avatars and a virtual object. It is important to note that the two parts of the algorithm are currently considered decoupled. This is not a fully accurate model of what happens in reality since the relationship that links P and M depends on the tangential forces being applied on the object [10, 12]. Given this assumption, in the following we will solely consider the evolution of angular variable α and its proxy value α_p.

When a soft finger avatar comes into contact with a virtual object α_p is set to the current value of the angle describing the rotation of the soft finger avatar α_0. The following steps are then performed until contact is not broken At a generic k-th time sample:

- The new angular position of the users fingers is calculated as $\alpha_g(K) = \alpha_s(K) - \alpha_p(K-1)$, where α_s is measured by the haptic device. α_g is the new goal value for α.

- α_p new value is computed as

$$\alpha_p(K) = \alpha_p(K-1) + \beta(K) \tag{38}$$

where

$$\beta(K) = 0 \quad \text{if} \quad |P(K)|^\gamma \mu_m > |M(K)| \tag{39}$$

and

$$\beta(K) = \alpha_g(K) - \alpha_p(K-1) - \frac{|P(K)|^\gamma \mu_d}{k_\tau} \quad \text{otherwise} \tag{40}$$

where P is the force along the contact normal, μ_m and μ_d are the coefficients of static and dynamic torsional friction between virtual object and user, γ depends on the model chosen for the rotational friction, $M(K) = k_\tau(\alpha_p(K-1) - \alpha_g(K))$ represents the torque applied to the object due to torsional friction, and k_τ is the haptic servo-loop gain. Note that μ_d can be picked to be smaller than μ_m. Experimental values of μ_d are currently under investigation.

- A new torque $M(K) = k_\tau(\alpha_p(K) - \alpha_g(K))$ is computed using the new value of α_p. Torque $M(K)\,\vec{v}_n$ is applied to the virtual object (where $\vec{v}_n$ represents a unit vector with direction along the contact normal). A torque $M(K)$ is also applied to the user (if the device used is capable of actuating such wrench).

- New velocity $(\vec{v}, \vec{\omega})$ and position $(\vec{x}, \vec{\theta})$ is computed for the virtual object. Angle α_c representing how much the object has rotated about axis $\vec{v}_n$ is computed as

$$\alpha_c = |\vec{\omega} \cdot \vec{v}_n|\, \Delta_T \tag{41}$$

where Δ_T is the servo-loop sampling time.

- The current value of α_p is corrected to

$$\alpha_p = \alpha_p + \alpha_c \tag{42}$$

8. Applications

The algorithm proposed in section has been used in conjunction with a dual-handed haptic device allowing two-point interaction with virtual object per hand (see Figure 11). The current design of the device does not allow to recreate contact torques on the users' fingertips. In this scenario the soft-finger algorithm is used solely to compute the effect of the user on the virtual environment. Work is currently being carried out in order to add rotational feedback on the user's fingertips.

Figure 11. Manipulating virtual objects using two fingers per hand.

9. Conclusions

In this paper we consider four possible models for in-vivo human fingerpad. For each of such models we obtain a relationship between contact force and torque due to rotational friction. Such models are compared. The model based on liquid filled membrane turns out to be the most complete and precise. However if some of the parameters that characterize the models are not considered, such as the contact surface in the case of point-based algorithms, then all models turn out to give very similar rotational friction relationships. A proxy-based algorithm that models soft finger contact is also proposed. It is important to note that algorithm considers tangential forces and rotational forces to be decoupled. This is an approximation of what happens in reality. Work is being carried out in order to remove such limitation.

References

[1] C. Avizzano, T. Gutierrez, S. Casado, B. Gallagher, M. Magennis, J. Wood, K. Gladstone, H. Graupp, J. A. Munoz, E. F. C. Arias, and F. Slevin. Grab: Computer graphics access for blind people through a haptic and audio virtual environment. In *Proceedings of Eurohaptics 2003*, July 2003.

[2] F. Barbagli, R. DeVengenzo, and K. Salisbury. Dual-handed virtual grasping. In *submitted to the 2003 IEEE International Conference on Robotics and Automation, ICRA 2003*, volume 1, pages 1259–1263, Taipei, Taiwan, 2003.

[3] D. Brock. Enhancing the dexterity of a robot hand using controlled slip. In *Proceedings of the IEEE International Conference on Robotics and Automation*, volume 1, pages 249–251, 1988.

[4] P. Dupont, V. Hayward, B. Armstrong, and F. Altpeter. Single state elasto-plastic friction models. *IEEE Transactions on Automatic Control*, 47(5):787–792, 2002.

[5] A. W. Goodwin, P. Jenmalm, and R. S. Johansson. Control of grip force when tilting objects: Effect of curvature of grasped surfaces and applied tangential torque. *J. Neuroscience*, 18(24):10724–10734, 1998.

[6] A. E. Green and J. E. Adkins. *Large elastic deformatoins*. Oxford at Clarendon Press, 1960.

[7] H. C. Guler, N. Berme, and S. R. Simon. A viscoelastic sphere model for the representation of plantar soft tissue during simulation. *Journal of Biomechanics*, 31:847–53, 1998.

[8] H. Hertz. On the contact of elastic solids. *J. Reine und angewandte Mathematik*, 92:156–171, 1882. (for english translation see *Miscellaneous Papers by H. Hertz*, Eds Jones and Schott, London: Macmillan 1896).

[9] R. Howe, I. Kao, and M. Cutkosky. The sliding of robot fingers under combined torsion and shear loading. volume 1, pages 103–105, 1988.

[10] R. D. Howe and M. R. Cutkosky. Practical force-motion models for sliding manipulation. *International Journal of Robotic Resarch*, 15:557–572, 1996.

[11] K. Johnson. *Contact Mechanics*. Cambridge University Press, 1985.

[12] H. Kinoshita, L. Backstrom, J. R. Flanagan, and R. S. Johansson. Tangential torque effects on the control of grip forces when holding objects with a precision grip. *J. Neurophysiol.*, (78):1619–1630, 1998.

[13] A. Nahvi and J. Hollerbach. Display of friction in virtual environments based on human finger pad characteristics. In *Proceedings of ASME Dynamic Systems and Control Division*, volume DSC-Vol. 64, pages 179–184, November 1998.

[14] D. Pawluk and R. Howe. Dynamic contact of the human fingerpad against a flat surface. *Journal of Biomechanical Engineering*, 121:605–611, 1999.

[15] D. Pawluk and R. Howe. Dynamic lumped element response of the human fingerpad. *Journal of Biomechanical Engineering*, 121:178–183, 1999.

[16] D. C. Ruspini, K. Kolarov, and O. Khatib. The haptic display of complex graphical environments. In *Computer Graphics (SIGGRAPH 97 Conference Proceedings)*, pages 345–352. ACM SIGGRAPH, 1997.

[17] K. Salisbury and Mason. *Robot Hands and the Mechanics of Manipulation*. MIT press, 1985.

[18] E. Serina, , C. Mote, and D. Rempel. Force response of the fingertip pulp to repeated compression: Effects of loading rate, loading angle, antropometry. *Journal of Biomechanics*, 30:1035–1040, 1997.

[19] E. Serina, E. Mockensturm, C. Mote, and D. Rempel. A structural model of the forced compression of the fingertip pulp. *Journal of Biomechanics*, 31:639–646, 1998.

[20] M. Srinivasan and K. Dandekar. An investigation of the mechanics of tactile sense using two dimensional models of the primate fingertip. *Journal of Biomechanical Engineering*, 118:48–55, 1996.

[21] G. Westling and R. S. Johansson. Factors influencing the force control during precision grip. *Experimental Brain Research*, (53):277–284, 1998.

[22] C. Zilles and J. Salisbury. A constraintbased god-object method for haptic display. In *Proc. IEE/RSJ International Conference on Intelligent Robots and Systems, Human Robot Interaction, and Cooperative Robots*, volume 3, pages 146–151, 1995.